Supporting Online Material for

Controlling Chemical Self-Assembly by Solvent-Dependent Dynamics

Peter A. Korevaar, Charley Schaefer, Tom F. A. de Greef* and E. W. Meijer*

* To whom correspondences should be addressed: t.f.a.d.greef@tue.nl, e.w.meijer@tue.nl.

Contents

Experimental Section

Solvents were obtained from Sigma-Aldrich (methylcylohexane, spectrophotometric grade, 99%) and Biosolve (chloroform, AR, > 99.9%) and used as received.

Circular dichroism (CD) spectra were recorded using a Jasco J-815 CD spectrometer. Sensitivity, response time and scanning rate were chosen appropriately. The temperature was controlled using a Jasco Peltier temperature controller with a range of 263–383 K and adjustable temperature slope. Molar ellipticity $\Delta\varepsilon$ in [1/M·cm] was found via $\Delta\varepsilon$ = CD [mdeg] / (32982 x concentration OPV [M] x optical pathlength [cm]). UV-vis spectra were recorded using a Jasco V-650 UV-vis spectrometer. The temperature was controlled using a Jasco Peltier temperature controller with a range of 263–383 K and adjustable temperature slope. Stopped-flow studies were performed using a Biologic SFM 400 stopped-flow setup with Berger Ball mixer, Biologic TC 100 cuvet (optical path length 1 mm or 1 cm), and Biologic MPS-60 controller unit. The stopped-flow as connected in-line with a Jasco J-815 CD spectrometer. To control the temperature of cuvet and syringes, SFM 400 was connected to a Julabo F12 temperature controller (ethylene glycol bath with thermostat). The mixing efficiency was assessed as described in ref. S4.

The kinetic experiments on the depolymerization of OPV described in Figure 2 and 3 are performed by manually mixing of the solutions of OPV in chloroform and OPV in MCH. The experiments are conducted in quartz cuvettes with optical path lengths of 1 cm (12 μM), 5 mm (24 μM) and 1 mm (63 μM).

The stopped-flow experiments on the depolymerization kinetics of OPV are performed with mixing times < 10 ms, mixing volumes, rates and ratios were chosen appropriately. The depolymerization was followed in time with CD (λ = 466 nm, $\Delta\lambda$ = 1 nm, Δt = 1 s, standard sensitivity, high tension voltage adjusted to get a direct-current voltage around 1 V). The duration of the measurements was adjusted appropriately.

Numerical simulations on the kinetic model, and simulations and curve fitting with the equilibrium model were performed using Matlab 7.9.0 R2009b.

Supporting Data

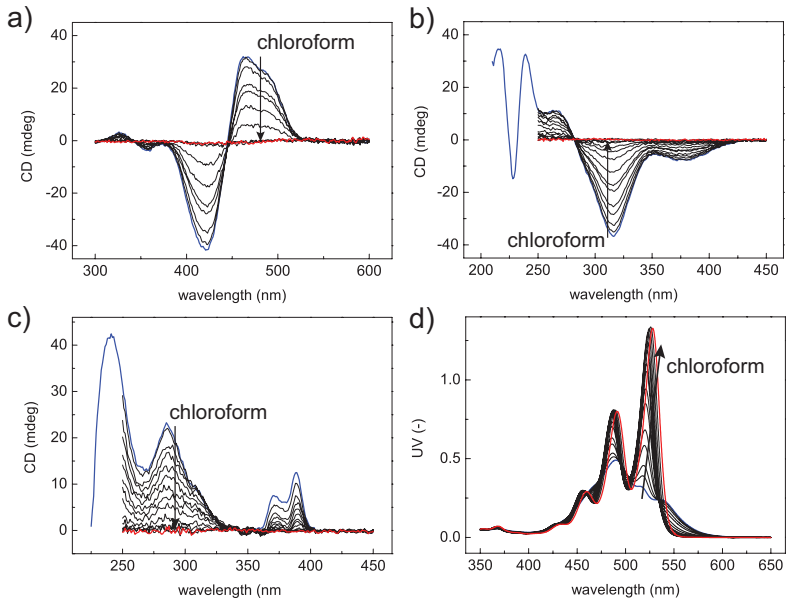

Figure S1. CD (a, b, c) and UV-vis (d) spectra of *R*-chiral oligo(*p*-phenylene vinylene)-ureidotriazine (OPV) **1** (a, 24 μM, *l* = 5 mm), *S*-chiral benzene-1,3,5-trithioamide **2** (b, 19 μM, *l* = 1 cm), *R*-chiral 3,3'-diamino-2,2'-bipyridine C_3-discotic **3** (c, 14 μM, *l* = 1 cm) and perylene tetracarboxylic acid bisimide **4** (d, 146 μM, *l* = 1 mm) at 20 °C in MCH with increasing chloroform volume fraction along the arrow. The spectra in pure MCH and pure chloroform are depicted in blue and red, respectively.

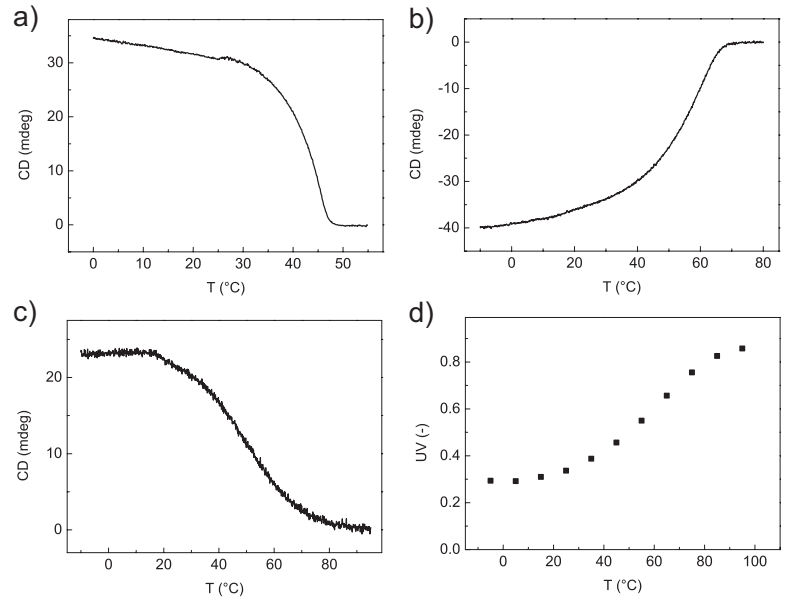

Figure S2. Temperature-dependent CD (a, b, c) and UV-vis (d) of **1** (a, 24 μM, 466 nm, *l* = 5 mm, 4 K/hr), **2** (b, 19 μM, 316 nm, *l* = 1 cm, 60 K/hr), **3** (c, 14 μM, 286 nm, *l* = 1 cm, 60 K/hr) and **4** (d, 146 μM, 513.5 nm, *l* = 1 mm) in MCH.

Details of supramolecular polymerization equilibrium model.

To describe the denaturation data we use the concentration-dependent supramolecular polymerization equilibrium model as first analyzed by Goldstein and Stryer (ref. S1). The model, which is also derived in the Supplementary Information of ref. S4, describes the supramolecular polymerization as a sequence of monomer addition equilibria:

$$\begin{aligned}
&\mathrm{X} + \mathrm{X} \overset{K_\mathrm{n}}{\longleftrightarrow} \mathrm{P}_2 && \left[\mathrm{P}_2\right] = K_\mathrm{n}\left[\mathrm{X}\right]^2 \\
&\mathrm{P}_2 + \mathrm{X} \overset{K_\mathrm{n}}{\longleftrightarrow} \mathrm{P}_3 && \left[\mathrm{P}_3\right] = K_\mathrm{n}\left[\mathrm{P}_2\right]\left[\mathrm{X}\right] \\
&\quad\vdots \\
&\mathrm{P}_{\mathrm{n}-1} + \mathrm{X} \overset{K_\mathrm{n}}{\longleftrightarrow} \mathrm{P}_\mathrm{n} && \left[\mathrm{P}_\mathrm{n}\right] = K_\mathrm{n}\left[\mathrm{P}_{\mathrm{n}-1}\right]\left[\mathrm{X}\right] \\
&\mathrm{P}_\mathrm{n} + \mathrm{X} \overset{K_\mathrm{e}}{\longleftrightarrow} \mathrm{P}_{\mathrm{n}+1} && \left[\mathrm{P}_{\mathrm{n}+1}\right] = K_\mathrm{e}\left[\mathrm{P}_\mathrm{n}\right]\left[\mathrm{X}\right] \\
&\quad\vdots \\
&\mathrm{P}_{\mathrm{i}-1} + \mathrm{X} \overset{K_\mathrm{e}}{\longleftrightarrow} \mathrm{P}_\mathrm{i} && \left[\mathrm{P}_\mathrm{i}\right] = K_\mathrm{e}\left[\mathrm{P}_{\mathrm{i}-1}\right]\left[\mathrm{X}\right]. \\
&\quad\vdots
\end{aligned} \tag{S1}$$

In case of a cooperative supramolecular polymerization, $K_\mathrm{n} < K_\mathrm{e}$ (with K_n the equilibrium constant of nucleation, K_e the equilibrium constant of elongation and with cooperativity $\sigma = K_\mathrm{n} / K_\mathrm{e}$). Obviously, in an isodesmic supramolecular polymerization, $K_\mathrm{n} = K_\mathrm{e}$ ($\sigma = 1$). The concentration of each species P_i equals $[\mathrm{P}_\mathrm{i}] = K_\mathrm{n}^{i-1}[\mathrm{X}]^i$ for $i \le n$ and $[\mathrm{P}_\mathrm{i}] = K_\mathrm{e}^{i-n}K_\mathrm{n}^{n-1}[\mathrm{X}]^i$ for $i > n$. With dimensionless concentration $p_\mathrm{i} = K_\mathrm{e}[\mathrm{P}_\mathrm{i}]$, dimensionless monomer concentration $x = K_\mathrm{e}[\mathrm{X}]$, the dimensionless concentration of each species P_i equals $p_\mathrm{i} = \sigma^{i-1}x^i$ for $i \le n$ and $p_\mathrm{i} = \sigma^{n-1}x^i$ for $i > n$. Hence, the dimensionless mass balance is

$$x_\mathrm{tot} = \sigma^{-1}\sum_{i=1}^{n} i\left(\sigma x\right)^i + \sigma^{n-1}\sum_{i=n+1}^{\infty} i x^i \,. \tag{S2}$$

with dimensionless total concentration $x_\mathrm{tot} = K_\mathrm{e}c_\mathrm{tot}$ and c_tot the total monomer concentration in mol/L.

Evaluating both sums in eq. S2 using standard expressions for converging series yields:

$$x_\mathrm{tot} = \sigma^{-1}\left(\frac{\left(\sigma x\right)^{n+1}\left(n\sigma x - n - 1\right)}{\left(\sigma x - 1\right)^2} + \frac{\sigma x}{\left(\sigma x - 1\right)^2}\right) - \sigma^{n-1}\left(\frac{x^{n+1}\left(nx - n - 1\right)}{\left(x - 1\right)^2}\right). \tag{S3}$$

Solving eq. S3 using standard numerical methods (Matlab *fzero* solver) yields the dimensionless monomer concentration x. Subsequently, if all species with $i > 1$ are considered as aggregates the degree of aggregation φ can be found via:

$$\varphi = \frac{x_{\mathrm{tot}} - x}{x_{\mathrm{tot}}}. \tag{S4}$$

In the case of OPV assembly however, the CD signal is assumed to originate from solely post-nucleus aggregates.[S2] Hence, we consider the degree of aggregation for OPV to be equal to:

$$\varphi = \frac{x_{\mathrm{tot}} - x - \sum_{2}^{n} i \cdot p_{\mathrm{i}}}{x_{\mathrm{tot}}}. \tag{S5}$$

The denaturation curves are calculated via $K_{\mathrm{e}} = \exp(-\Delta G^{0\prime}/RT)$, where the dependence of Gibbs free energy of monomer association $\Delta G^{0\prime}$ on the chloroform volume fraction f is defined via:

$$\Delta G^{0\prime} = \Delta G^{0} + m \cdot f \tag{S6}$$

The cooperativity parameter σ is assumed to be independent of f, *i.e.* the m-value involved in the nucleation Gibbs free energy equals the m-value involved in further elongation.

To assess the influence of ΔG^{0}, m, σ and c_{tot} on the denaturation curves, simulations are performed. As shown in Figure S3, decreasing σ results in an increasing sharpness of the curve around the critical point, (f_{crit}). Increasing the m-value results in a decreasing value for the critical chloroform volume fraction f_{crit}. Both increasing c_{tot} as well as $-\Delta G^{0}$ results in an increasing f_{crit}. Since $\Delta G^{0} = \Delta H^{0} - T\Delta S^{0}$, it can be concluded that for enthalpy driven supramolecular polymerizations (with $\Delta H^{0} < 0$ and $\Delta S^{0} < 0$) decreasing the temperature results in an increasing value of f_{crit}, as observed experimentally (Figure 1d).

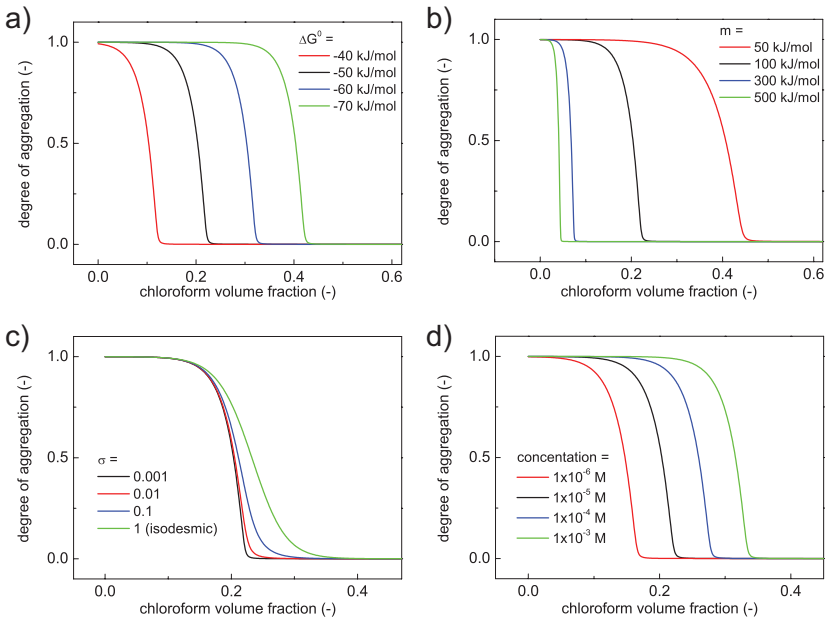

Figure S3. Simulated influence of ΔG^0 (a), m (b), σ (c) and c_{tot} (d) on degree of aggregation *vs*. chloroform volume fraction (ΔG^0 = –50 kJ/mol, m = 100 kJ/mol, σ = 0.001, c_{tot} = 10 µM, n = 2, T = 293 K, unless stated differently).

To fit the supramolecular polymerization equilibrium model to the denaturation data acquired on the supramolecular polymers **1** – **4**, the normalized degree of aggregation is deduced from the changes observed in CD or UV-vis. For **1 – 3**,

$$\text{normalized degree of aggregation } (f) = \frac{\text{CD}(f)}{\text{CD}(f=0)}, \tag{S7}$$

for **4**,

$$\text{normalized degree of aggregation } (f) = \frac{\text{UV-vis}(f) - \text{UV-vis}(f=0)}{\text{UV-vis}(f=1) - \text{UV-vis}(f=0)}. \tag{S8}$$

It should be mentioned that the normalized degree of aggregation obtained via eq. S7 and S8 equals 1 in pure MCH (f = 0). However, if the experimental CD or UV-vis value obtained in pure MCH is not yet saturated at the temperature at which the experiment is performed, a normalization factor p should be introduced to match the normalized degree of aggregation (eq. S7, S8) and the calculated degree of aggregation φ (eq. S4, S5).

Taken together, four parameters need to be optimized to fit the equilibrium model to the data (normalized degree of aggregation *vs*. *f*): ΔG^0, m, σ and p. The optimized parameters are found via a non-linear least-squares analysis where the sum of the squared residuals is minimized using Matlab (*lsqnonlin* solver). The data are fitted with non-linear least squared regression, using the Levenberg-Marquardt algorithm. To analyze the data acquired at multiple concentrations in one curve fitting procedure, the sum of all squared residuals is minimized using the same procedure. To avoid the program getting trapped in a local minimum, 100 different initial parameter sets are defined, and the best fit is taken as the final solution for

the values of ΔG^0, m, σ and p. The different initial parameter sets are defined using a *latin hypercube sampling* method (Matlab function *lhsdesign*). Initial parameter values are in the intervals $\Delta G^0 \in$ [-50, -20] kJ/mol, $m \in$ [50, 120] kJ/mol, $\sigma \in$ [0, 1] and $p \in$ [0.9, 1.1], the boundaries are adjusted if necessary. The results of the curve fitting procedure are shown in Table S1.

Tabel S1. Results of fitting equilibrium model to denaturation curves.

compound	**concentration** (μM)	**Temperature** (°C)	ΔG^0 (kJ/mol)	m (kJ/mol)	σ (-)	p (-)
1	12	20	$-36 \pm 1 \cdot 10^5$	75 ± 4	$0 \pm 2 \cdot 10^4$	1.06 ± 0.02
1	12	20	-37.5 ± 0.4	83 ± 5	0.16*	1.04 ± 0.02
1	24	20	-37.1 ± 0.4	83 ± 3	0.16 ± 0.03	1.023 ± 0.008
1	63	20	-39 ± 3	$(1.0 \pm 0.2) \cdot 10^2$	0.2 ± 0.2	0.97 ± 0.03
1	12	10	$-36 \pm 1 \cdot 10^6$	57 ± 7	$0 \pm 2 \cdot 10^5$	1.03 ± 0.03
1	12	10	-37.0 ± 0.4	62 ± 4	0.16*	1.02 ± 0.02
2	19	20	-31.5 ± 0.5	29 ± 3	$(8 \pm 8) \cdot 10^{-4}$	1.14 ± 0.05
3	14	20	-32.7 ± 0.3	81 ± 2	1**	1.09 ± 0.01
4	146	20	-24.0 ± 0.5	58 ± 3	1**	1.27 ± 0.05

* The value of σ is fixed at 0.16 to avoid problems with accurate determination of ΔG^0.
** The value of σ is fixed at 1 in the analysis of the denaturation of isodesmic systems **3** and **4**.

The large standard deviations found for the values of ΔG^0 and σ for the denaturation of **1** at 12 μM (10 °C and 20 °C) can be rationalized by the fact that in these denaturation curves data points are lacking around the critical chloroform volume fraction. Especially this region of the denaturation curve is very dependent on σ, as shown in Figure S3c, and hence – vice versa – of importance for an accurate determination of the value of σ via the curve fitting procedure. Indeed, if σ is fixed during the curve fitting procedure, ΔG^0 can be determined with a much higher accuracy, as shown in Table S1.

Moreover, the accuracy of the parameter values determined via the fitting procedure depends on the correlation between the different parameters, which is a measure for the influence that a change in the value of one parameter (e.g. ΔG^0) has on the value of another parameter (e.g. σ) that is found via the fitting procedure.[S3] First, the covariance matrix *Cov* is found via:

$$Cov = \frac{resnorm}{\#DOF}\left(Jacobian^T \cdot Jacobian\right)^{-1}, \tag{S9}$$

where *resnorm* is the sum of the normalized residuals in the fitting procedure, *#DOF* is the number of degrees of freedom (which equals the number of data points minus the number of fitting parameters). The *Jacobian* is a matrix in which the number of columns is given by the number of free parameters and the number of rows equals the number of datapoints. Each element $Jacobian_{ij}$ represents the derivative of the residual for datapoint i to parameter j. The standard deviation of each parameter i can be found by taking the square root of Cov_{ii}.

Subsequently, the elements of the correlation matrix *Corr* (Pearson correlation coefficients) are obtained via:

$$Corr_{ij} = \frac{Cov_{ij}}{\sqrt{Cov_{ii} Cov_{jj}}}. \quad \text{(S10)}$$

The off-diagonal values $Corr_{ij}$ (with $i \neq j$) represent the correlation between parameter i and j, with $Corr_{ij} = 0$ indicating no correlation and $C_{ij} = \pm 1$ indicating maximum correlation. Obviously, $Corr_{ij} = Corr_{ji}$, and $Corr_{ii} = 1$. The correlation matrices for the different fits in Table S1 are given below:

Table S2. Correlation matrix for fit on denaturation of **1**, 12 μM, 20 °C: σ fitted (top), σ fixed (bottom).

	ΔG^0	m	σ	p
ΔG^0	1	0.01153	–1.00000	–0.00740
m		1	–0.01153	–0.88051
σ			1	0.00740
p				1

	ΔG^0	m	p
ΔG^0	1	–0.99678	0.86870
m		1	–0.84899
p			1

Table S3. Correlation matrix for fit on denaturation of **1**, 24 μM, 20 °C.

	ΔG^0	m	σ	p
ΔG^0	1	–0.98163	–0.86417	0.77290
m		1	0.75659	–0.81919
σ			1	–0.46801
p				1

Table S4. Correlation matrix for fit on denaturation of **1**, 63 μM, 20 °C.

	ΔG^0	m	σ	p
ΔG^0	1	–0.99264	–0.86335	0.70776
m		1	0.79907	–0.73516
σ			1	–0.43457
p				1

Table S5. Correlation matrix for fit on denaturation of **1**, 12 μM, 10 °C (top) σ fitted (bottom) σ fixed.

	ΔG^0	m	σ	p
ΔG^0	1	–0.89260	–1.00000	0.69774
m		1	0.89260	–0.90759
σ			1	–0.69774
p				1

	ΔG^0	m	p
ΔG^0	1	–0.99498	0.87532
m		1	–0.85099
p			1

Table S6. Correlation matrix for fit on denaturation of **2**, 19 μM, 20 °C.

	ΔG^0	m	σ	p
ΔG^0	1	–0.99346	–0.75420	0.96284
m		1	0.81781	–0.94190
σ			1	–0.67376
p				1

Table S7. Correlation matrix for fit on denaturation of **3**, 14 μM, 20 °C.

	ΔG^0	m	p
ΔG^0	1	–0.96991	0.90463
m		1	–0.81463
p			1

Table S8. Correlation matrix for fit on denaturation of **4**, 146 μM, 20 °C.

	ΔG^0	m	p
ΔG^0	1	–0.96614	0.97529
m		1	–0.90839
p			1

The problem of insufficient data around the critical solvent composition together with high correlation between parameters can be solved by performing the curve fitting simultaneously on three different denaturation curves acquired at different concentrations (**1**, 12 μM, 24 μM and 63 μM, 20 °C). The values of ΔG^0, m and σ are assumed to be concentration-independent and individual normalization factors p_1, p_2 and p_3 are used for the three different curves. The obtained fit, shown in Figure 1c of the main text, results in the following parameter values:

Tabel S9. Results of fitting the equilibrium model to multiple denaturation curves of **1**.

ΔG^0 (kJ/mol)	m (kJ/mol)	σ (-)	p_1 (-)	p_2 (-)	p_3 (-)
–39.9 ± 0.4	109 ± 3	0.25 ± 0.04	0.96 ± 0.01	0.99 ± 0.02	0.98 ± 0.02

No large standard deviations are obtained, and also the correlation matrix shows lower correlation values, indicating that more accurate values can be obtained by curve fitting multiple denaturation data sets acquired at different concentrations.

Table S10. Correlation matrix for fit on multiple denaturation curves of **1**, 20 °C.

	ΔG^0	m	σ	p_1	p_2	p_3
ΔG^0	1	–0.93624	–0.73729	–0.15980	0.38164	0.13231
m		1	0.47829	0.12000	–0.46083	–0.20712
σ			1	0.26403	0.00394	0.15344
p_1				1	0.07485	0.11034
p_2					1	0.24607
p_3						1

The values of ΔG^0 and σ that are obtained via fitting the equilibrium model to the denaturation curves of OPV at multiple concentrations are verified with values of ΔG^0 and σ following from the analysis of temperature-dependent data. As shown in Figure S4, cooling curves of OPV acquired at concentrations of 24 μM and 102 μM are fitted with the equilibrium model that makes use of temperature-dependent equilibrium constants K_n and K_e. The temperature-dependency of K_n and K_e is defined via $K_n = \exp(-(\Delta H_n^0 - T{\cdot}\Delta S_n^0) / (R{\cdot}T))$ and $K_e = \exp(-(\Delta H_e^0 - T{\cdot}\Delta S_e^0) / (R{\cdot}T))$, with ΔH_n^0 and ΔH_e^0 the enthalpy of nucleation and elongation, respectively, ΔS_n^0 and ΔS_e^0 the entropy of nucleation and elongation, respectively, R the gas constant and T the temperature. The resulting values of ΔG^0 and σ at 20 °C are in good agreement with the values obtained via the denaturation experiments.

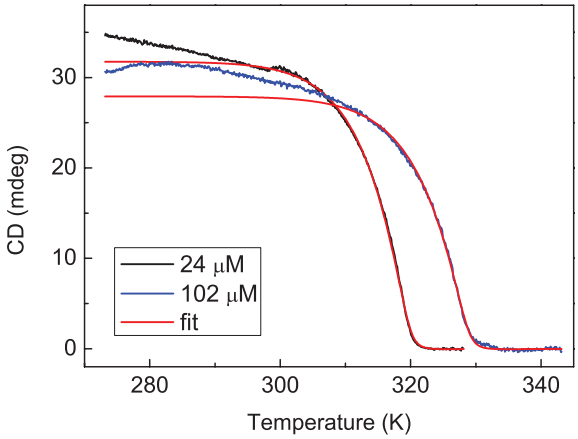

Figure S4. CD (466 nm) *vs.* temperature for **1** at 24 μM (optical pathlength l = 5 mm, 4 K/hr) and 102 μM (l = 1 mm, 60 K/hr) in MCH, fitted with temperature-dependent equilibrium model. Based on the obtained values for the enthalpies and entropies of nucleation and elongation (ΔH_e^0 = (–140.9 ± 0.3) kJ/mol, ΔS_e^0 = (–343.3 ± 0.9) J/K.mol, ΔH_n^0 = (–141 ± 0.3) kJ/mol, ΔS_n^0 = (–356.8 ± 0.9) J/K.mol), $\Delta G^0 = \Delta H_e^0 - T{\cdot}\Delta S_e^0$ = –40.4 kJ/mol and σ = 0.20 at 20 °C.

Fitting the denaturation data on cooperative systems **1** and **2** assuming isodesmic growth (*i.e.* fixing the value of σ to 1) gives a significant worse description of the data, as shown in Figure S5.

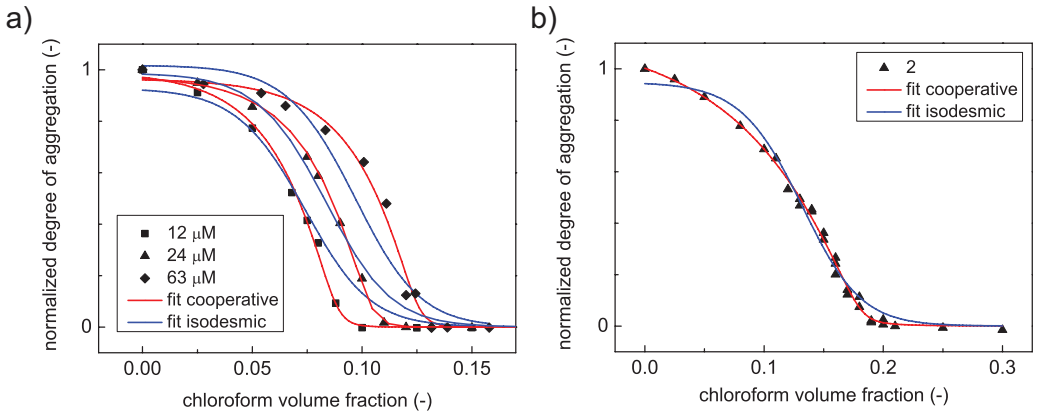

Figure S5. Fit of denaturation curve of **1** (a, 20 °C) and **2** (19 μM, 20 °C) with both the isodesmic (σ = 1) and cooperative supramolecular polymerization equilibrium model. The data acquired on the denaturation of **1** at multiple concentrations are fitted with concentration-independent values for ΔG^0 and m but with three normalization constants p_1, p_2 and p_3.

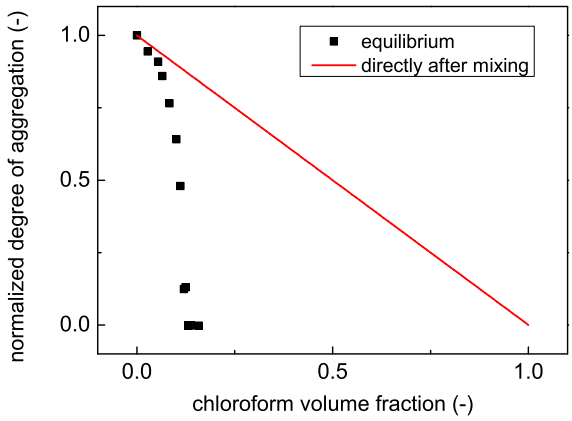

Figure S6. Normalized degree of aggregation *vs.* chloroform volume fraction for denaturation of **1** (63 μM, 20 °C) under equilibrium conditions, compared to the normalized degree of aggregation that is obtained directly after homogeneous mixing of **1** in MCH with **1** in chloroform. Directly after homogeneous mixing, the normalized degree of aggregation is expected to be on the line $y = 1 - f$, *i.e.* the weighted average of the normalized degree of aggregation in MCH ($1 \cdot (1 - f)$) and the normalized degree of aggregation in chloroform ($0 \cdot f$). At this concentration, for all data points the equilibrium normalized degree of aggregation is lower than the line $y = 1 - f$. This rules out the alternative explanation that the observed re-assembly in time is due to an equilibrium degree of aggregation that exceeds the line $y = 1 - f$.

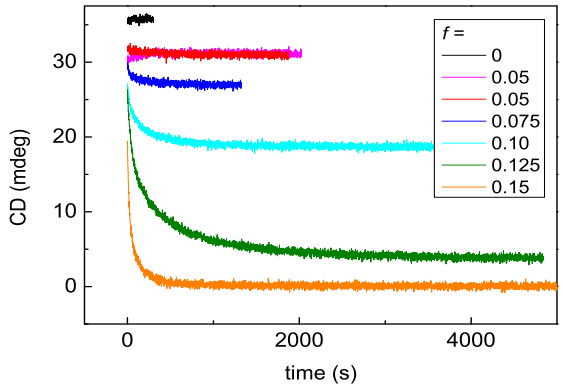

Figure S7. Depolymerization kinetics of OPV in MCH, induced by addition of OPV in chloroform at 10 °C (12 μM, manual mixing, l = 1 cm).

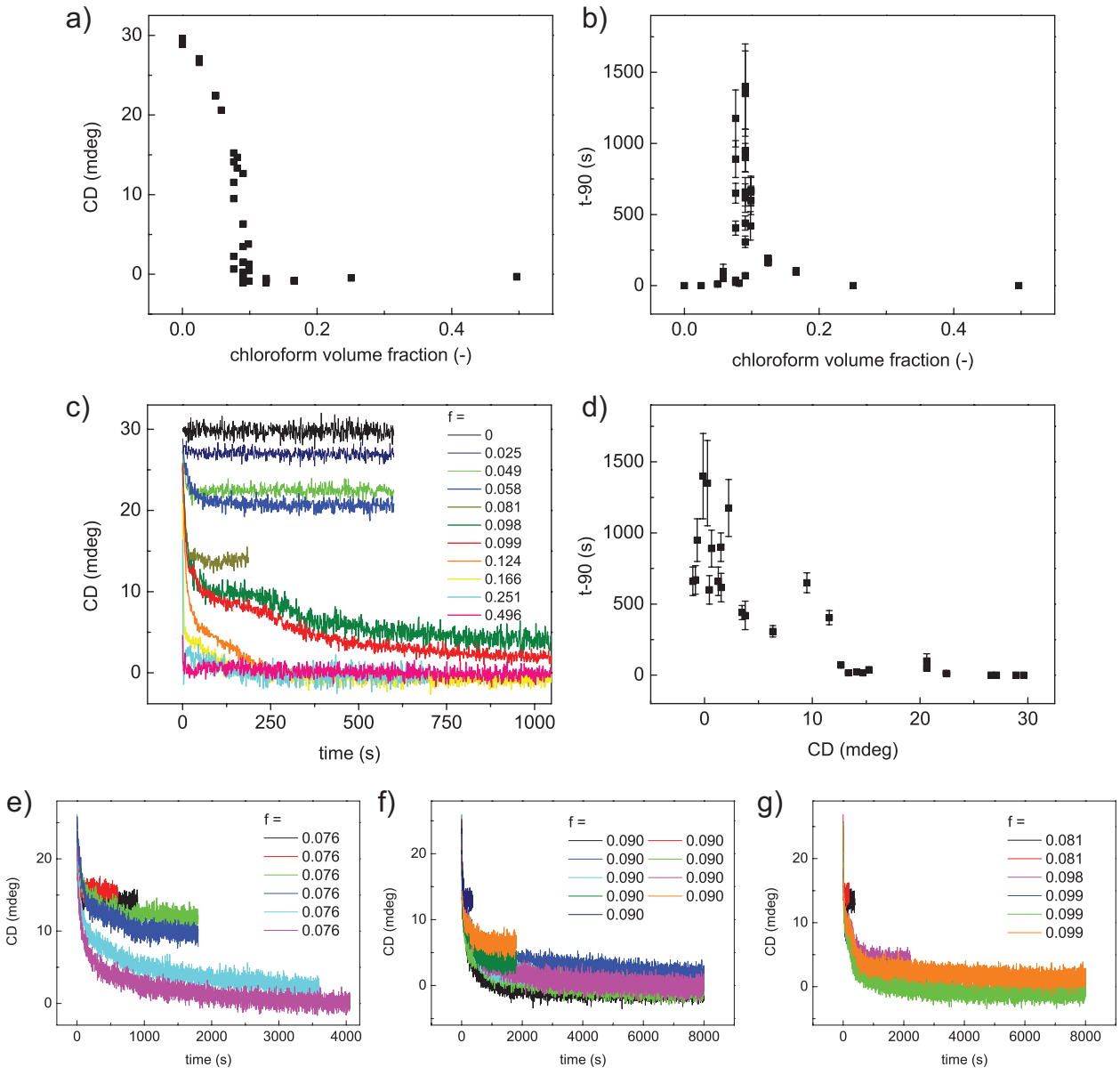

Figure S8. Stopped-flow experiments on depolymerization kinetics of **1** (12 μM, 20 °C, l = 1 cm). (a) CD values *vs.* chloroform volume fraction under equilibrium conditions. (b) *t*-90 *vs.* chloroform volume fraction. (c) Depolymerization kinetics at different chloroform volume fractions. The time-dependent curves are averaged over multiple injections (f = 0, 1x; f = 0.025, 2x; f = 0.049, 2x; f = 0.058, 2x; f = 0.081, 2x; f = 0.098, 1x; f = 0.099, 3x; f = 0.124, 5x; f = 0.166, 2x; f = 0.251, 2x; f = 0.496, 1x). The equilibrium CD values as well as the *t*-90 values show a large spreading around the critical chloroform volume fraction (f_{crit} ~ 0.1). This can be rationalized by the fact the value of f for each data point is derived from the mixing ratio of the MCH and chloroform solutions applied in each respective injection. However, close to the critical point, the final CD value and the rate are very dependent on the actual chloroform/MCH ratio, and a deviation by 1 percent can result in a difference of ~ 10 mdeg due to the steep slope of CD *vs.* f. The large influence of small variations in the mixing ratio obtained by the stopped-flow instrument

is illustrated by the time-dependent depolymerization traces obtained for several injections at $f = 0.076$ and $f = 0.09$, as shown in (e) and (f). For both mixing ratios, the curves with the smallest final CD value have the lowest rate. To further analyze this, for all injections with f between 0 and 0.099 the value of t-90 is analyzed in relation to the final CD value. As shown in (d), t-90 increases when the equilibrium CD value decreases. In addition to this trend, the rate increases again upon increasing the chloroform volume fraction beyond $f = 0.099$ (c). This demonstrates that also upon fast and efficient mixing in a stopped-flow instrument minimum depolymerization rates are obtained around the critical chloroform volume fraction.

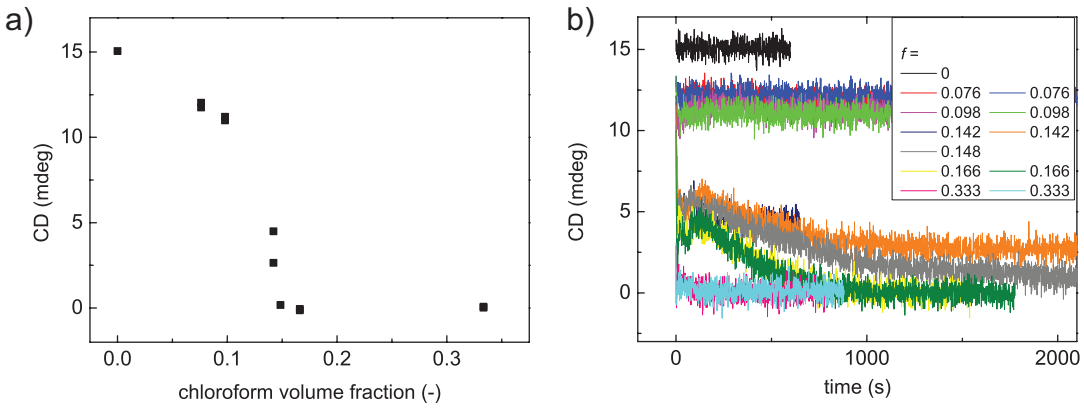

Figure S9. Stopped-flow experiments on depolymerization kinetics of **1** (51 µM, 20 °C, l = 1 mm). (a) CD values *vs.* chloroform volume fraction under equilibrium conditions. (b) Depolymerization kinetics at different chloroform volume fractions, revealing a minimum depolymerization rate around the critical chloroform volume fraction.

Details of supramolecular polymerization kinetics model.

In analogy to the model that we previously introduced in ref. S4 to describe the kinetics of a supramolecular polymerization process, we discuss here the details of the kinetic model that is used in the simulations on depolymerization and polymerization kinetics.

The reactions for the aggregation of monomer X are given by:

$$\begin{aligned}
&X + X \underset{b}{\overset{a}{\rightleftarrows}} P_2 \\
&P_2 + X \underset{b}{\overset{a}{\rightleftarrows}} P_3 \\
&\quad\vdots \\
&P_{n-1} + X \underset{b}{\overset{a}{\rightleftarrows}} P_n \\
&\quad\vdots \\
&P_{i-1} + X \underset{c}{\overset{a}{\rightleftarrows}} P_i .
\end{aligned} \tag{S11}$$

The kinetic model assumes that the aggregates can change size only by monomer association or dissociation. Furthermore, we assume that all forward rate constants are the same (a) and that the dissociation rate constants only differ between pre- and postnucleus aggregates (b and c, respectively), where the nucleus size is denoted by n. All aggregates up to a certain length N, with N much larger than the nucleus size n are described explicitly via differential equations. The aggregates with size larger than N are described together as fibrils by considering both the fibril number concentration,

$$[F] = [P_{N+1}] + [P_{N+2}] + [P_{N+3}] + \dots , \tag{S12}$$

and the fibril mass concentration,

$$[Z] = (N+1)[P_{N+1}] + (N+2)[P_{N+2}] + (N+3)[P_{N+3}] + \dots . \tag{S13}$$

In order to keep the fibril formation reversible, an estimation is needed for the number of fibrils of length N+1, the species that upon monomer dissociation results in the explicitly described aggregate of length N.

Assuming that for all $i > N$, $[\mathrm{P}_{i+1}] = \alpha[\mathrm{P}_i]$, one obtains

$$[\mathrm{F}] = \sum_{i=0}^{\infty} \alpha^i [\mathrm{P}_{N+1}],$$
$$[\mathrm{Z}] = \sum_{i=0}^{\infty} (N+1+i)\alpha^i [\mathrm{P}_{N+1}]. \tag{S14}$$

Using the standard series $\sum_{i=0}^{\infty} x^i = \frac{1}{1-x}$ and $\sum_{i=0}^{\infty} i \cdot x^i = \frac{x}{(x-1)^2}$ for $x < 1$, this yields

$$[\mathrm{F}] = [\mathrm{P}_{N+1}]\frac{1}{1-\alpha}, \qquad [\mathrm{Z}] = [\mathrm{P}_{N+1}]\left(\frac{N+1}{1-\alpha} + \frac{\alpha}{(1-\alpha)^2}\right). \tag{S15}$$

Substituting the equation for $[\mathrm{F}]$ in $[\mathrm{Z}]$ yields

$$[\mathrm{Z}] = [\mathrm{F}]\left(N+1+\frac{\alpha}{(1-\alpha)}\right), \tag{S16}$$

from which α can be solved as

$$\alpha = 1 - \frac{[\mathrm{F}]}{[\mathrm{Z}] - N[\mathrm{F}]}. \tag{S17}$$

The estimated concentration of aggregates of length N+1 is thus

$$[\mathrm{P}_{N+1}] = (1-\alpha)[\mathrm{F}]. \tag{S18}$$

The rate equations then become:

- for the monomers

$$\frac{\mathrm{d}[\mathrm{X}]}{\mathrm{d}t} = -a[\mathrm{X}]\left(2[\mathrm{X}] + \sum_{i=2}^{N}[\mathrm{P}_i] + [\mathrm{F}]\right) + b\left(2[\mathrm{P}_2] + \sum_{i=3}^{n}[\mathrm{P}_i]\right) + c\left(\sum_{i=n+1}^{N}[\mathrm{P}_i] + [\mathrm{F}]\right), \tag{S19}$$

- for the oligomers

$$\frac{\mathrm{d}[\mathrm{P}_i]}{\mathrm{d}t} = a[\mathrm{X}]\left([\mathrm{P}_{i-1}] - [\mathrm{P}_i]\right) + b\left([\mathrm{P}_{i+1}] - [\mathrm{P}_i]\right), \tag{S20}$$

- for the nucleus

$$\frac{\mathrm{d}[\mathrm{P_n}]}{\mathrm{d}t} = a[\mathrm{X}]\left([\mathrm{P_{n-1}}]-[\mathrm{P_n}]\right)+\left(c[\mathrm{P_{n+1}}]-b[\mathrm{P_n}]\right), \tag{S21}$$

- for polymers larger than the nucleus size *n*

$$\frac{\mathrm{d}[\mathrm{P_i}]}{\mathrm{d}t} = a[\mathrm{X}]\left([\mathrm{P_{i-1}}]-[\mathrm{P_i}]\right)+c\left([\mathrm{P_{i+1}}]-[\mathrm{P_i}]\right), \tag{S22}$$

- for the last explicitly considered aggregate with length *N*

$$\frac{\mathrm{d}[\mathrm{P_N}]}{\mathrm{d}t} = a[\mathrm{X}]\left([\mathrm{P_{N-1}}]-[\mathrm{P_N}]\right)+c\left((1-\alpha)[\mathrm{F}]-[\mathrm{P_N}]\right), \tag{S23}$$

- for the fibril number concentration

$$\frac{\mathrm{d}[\mathrm{F}]}{\mathrm{d}t} = a[\mathrm{X}][\mathrm{P_N}]-c(1-\alpha)[\mathrm{F}], \tag{S24}$$

- and for the fibril mass concentration

$$\frac{\mathrm{d}[\mathrm{Z}]}{\mathrm{d}t} = (N+1)\left(a[\mathrm{X}][\mathrm{P_N}]-c(1-\alpha)[\mathrm{F}]\right)+a[\mathrm{X}][\mathrm{F}]-c\left([\mathrm{F}]-(1-\alpha)[\mathrm{F}]\right), \tag{S25}$$

which can be rewritten into

$$\frac{\mathrm{d}[\mathrm{Z}]}{\mathrm{d}t} = a[\mathrm{X}]\left((N+1)[\mathrm{P_N}]+[\mathrm{F}]\right)-c\left([\mathrm{F}]+N(1-\alpha)[\mathrm{F}]\right). \tag{S26}$$

The resulting system of differential equations, combined with the relation between α, [F] and [Z] (eq. S17) is solved using the *ode15s* solver in Matlab.

To verify the assumption $[\mathrm{P_{i+1}}] = \alpha[\mathrm{P_i}]$ for $i > N$, we compare the concentration of monomers in stacks in the kinetic simulations under steady state conditions (*i.e* $\sum_{n+1}^{N} i\cdot[\mathrm{P_i}(t_{ss})]+[Z(t_{ss})]$ with the concentrations of monomer in stacks found via the equilibrium model (*i.e.* $\sum_{n+1}^{\infty} i\cdot[\mathrm{P_i}]$). t_{ss} represents the time corresponding to steady state conditions obtained via kinetic simulations. In this analysis, the

depolymerization kinetics are simulated assuming a solvent-dependency of the forward and backward rate constants a and c that is defined via:

$$\log(a) = \log(a^0) - m_a \cdot f\,; \tag{S27}$$

$$\log(c) = \log(c^0) + m_c \cdot f, \tag{S28}$$

respectively, with a^0 and c^0 the rate constants in pure MCH. Rate constant b is defined via

$$b = c/\sigma. \tag{S29}$$

The solvent-dependent equilibrium concentration of aggregated monomers is calculated via the solvent-dependent equilibrium constant of elongation $K_e = a / c$, with rate constants a and c defined via eq. S27 and S28, and equilibrium constant of nucleation $K_n = \sigma \cdot K_e$. As shown in Figure S10a, no differences in concentration of aggregated monomers *vs*. chloroform volume fraction are found between the equilibrium model and the steady state conditions following from the kinetic model. Furthermore, to verify the generality of the results found by simulation, we follow the time at which 25%, 50%, 70% and 80% of the conversion towards the equilibrium state is completed. As shown in Figure S10b, the resulting *t*-25, *t*-50, *t*-70 and *t*-80 show a dependence on the chloroform volume fraction similar to *t*-90.

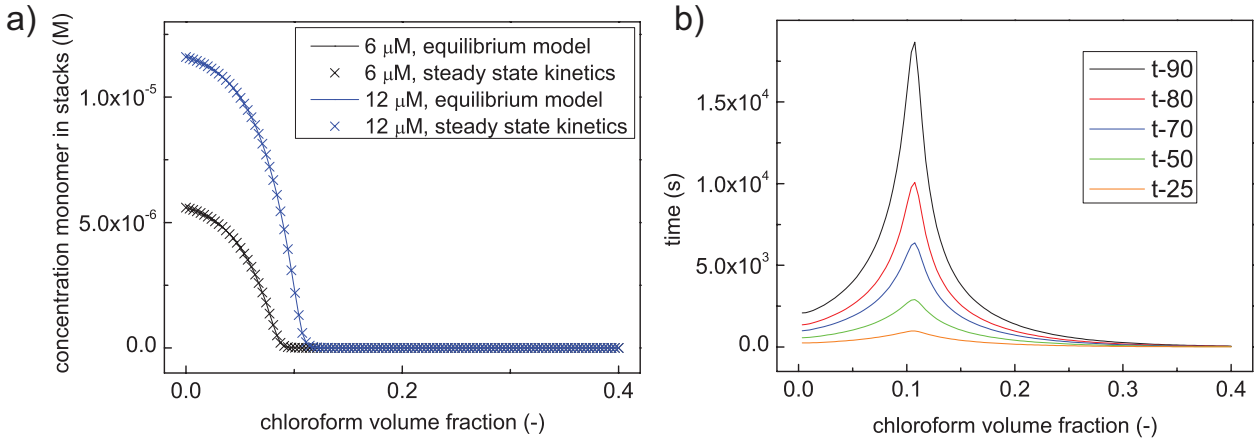

Figure S10. (a) The concentration of monomers in stacks under equilibrium conditions *vs.* chloroform volume fraction. The equilibrium concentrations are both found via the equilibrium model as well as via steady state conditions obtained upon kinetic simulations. (b) The time at which 25%, 50%, 70%, 80% and 90% (*t*-25, *t*-50, *t*-70, *t*-80 and *t*-90, respectively) of the conversion towards the equilibrium state is completed *vs*. chloroform volume fraction. ($a^0 = 6 \cdot 10^4$ $M^{-1}s^{-1}$, $c^0 = 1.71 \cdot 10^{-2}$ s^{-1}, $m_a = 7$, $m_c = 7$, $\sigma = 0.16$, $n = 5$, in b) OPV dimer concentration = 12 μM).

As demonstrated in ref. S4, the assembly of OPV can follow two pathways: a kinetically *vs.* thermodynamically controlled pathway that are competing for the same free monomer. However, in the analyses shown in this paper, only one assembly pathway is taken into account. To investigate the consequences of this simplification, we perform a depolymerization simulation that includes two assembly pathways, one thermodynamically controlled and one kinetically controlled. The kinetically controlled pathway results in an aggregate having opposite helicity (M-type) with lower stability (*i.e.* $K_e^* < K_e$) but a faster formation rate (*i.e.* $a^* > a$). Analogous to the procedure explained in the main text: first the equilibrium concentrations of monomer, oligomers and helical aggregates in pure MCH are calculated via the equilibrium model that includes only the thermodynamic pathway. Again, monomers that originate from the chloroform phase are added to the monomer pool, all concentrations are corrected for dilution due to mixing of the MCH and chloroform phases. Subsequently, the resulting concentrations for monomer, oligomers and each species P_i are taken as the starting condition for the simulation. Finally, the depolymerization kinetics are simulated at the respective chloroform/MCH ratio using these starting concentrations with rate constants for the thermodynamically controlled pathway defined via equations S27-29. The rate and equilibrium constants that characterize the kinetically controlled pathway are based on values used in ref. S4 to describe the aggregation of OPV. As shown in Figure S11, including the aggregation pathway resulting in metastable M-type aggregates yields higher values of *t*-90 and a slightly lower value of f_{crit} compared to simulations in which only one aggregation pathway is taken into account. However, the overall behavior remains the same, *i.e.* a minimum depolymerization rate is observed around the critical chloroform volume fraction. Hence, the comparable behavior with one or two aggregation pathways incorporated in the depolymerization simulations shows that the insights based on experimental observations on the depolymerization of OPV are not limited to systems that have metastable and thermodynamically stable states but can also be applicable to other supramolecular systems.

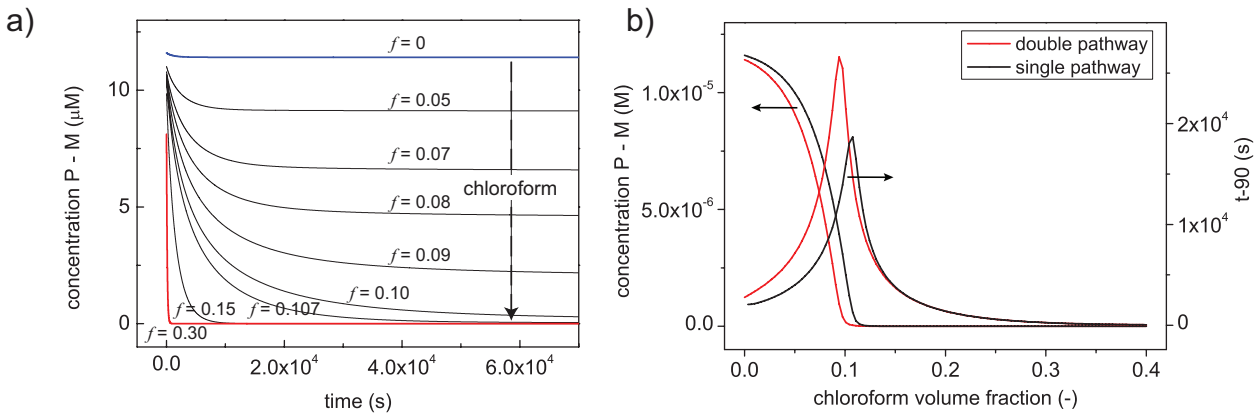

Figure S11. (a) Time-dependent concentration of monomers in thermodynamically stable P-stacks minus concentration of monomers in metastable M-stacks (P – M) during depolymerization of P-stacks with increasing amounts of chloroform. The initial concentrations of all P_i species are calculated via the equilibrium model, the disassembly kinetics are simulated via the kinetic model assuming two parallel operating self-assembly pathways as introduced in ref. S4. The pathway towards thermodynamically stable P-type assemblies is simulated with parameters $a^0 = 6 \cdot 10^4$ $M^{-1}s^{-1}$, $c^0 = 1.71 \cdot 10^{-2}$ s^{-1}, $m_a = 7$, $m_c = 7$, $\sigma = 0.16$ and $n = 5$. In agreement with simulations reported in ref. S4, the parameters that describe the metastable pathway (denoted with an asterisk *) are defined via $a^* / a = 3.79$, $K_n^* / K_n = 1.38$, $K_e^* / K_e = 0.164$, $n^* = 5$. The resulting values of t-90 and the concentration of monomers in P-stacks minus the concentration of monomers M-stacks (P – M) under equilibrium conditions (*i.e.* the steady state concentrations obtained via kinetic simulations) are plotted as a function of f in (b) (OPV dimer concentration 12 μM).

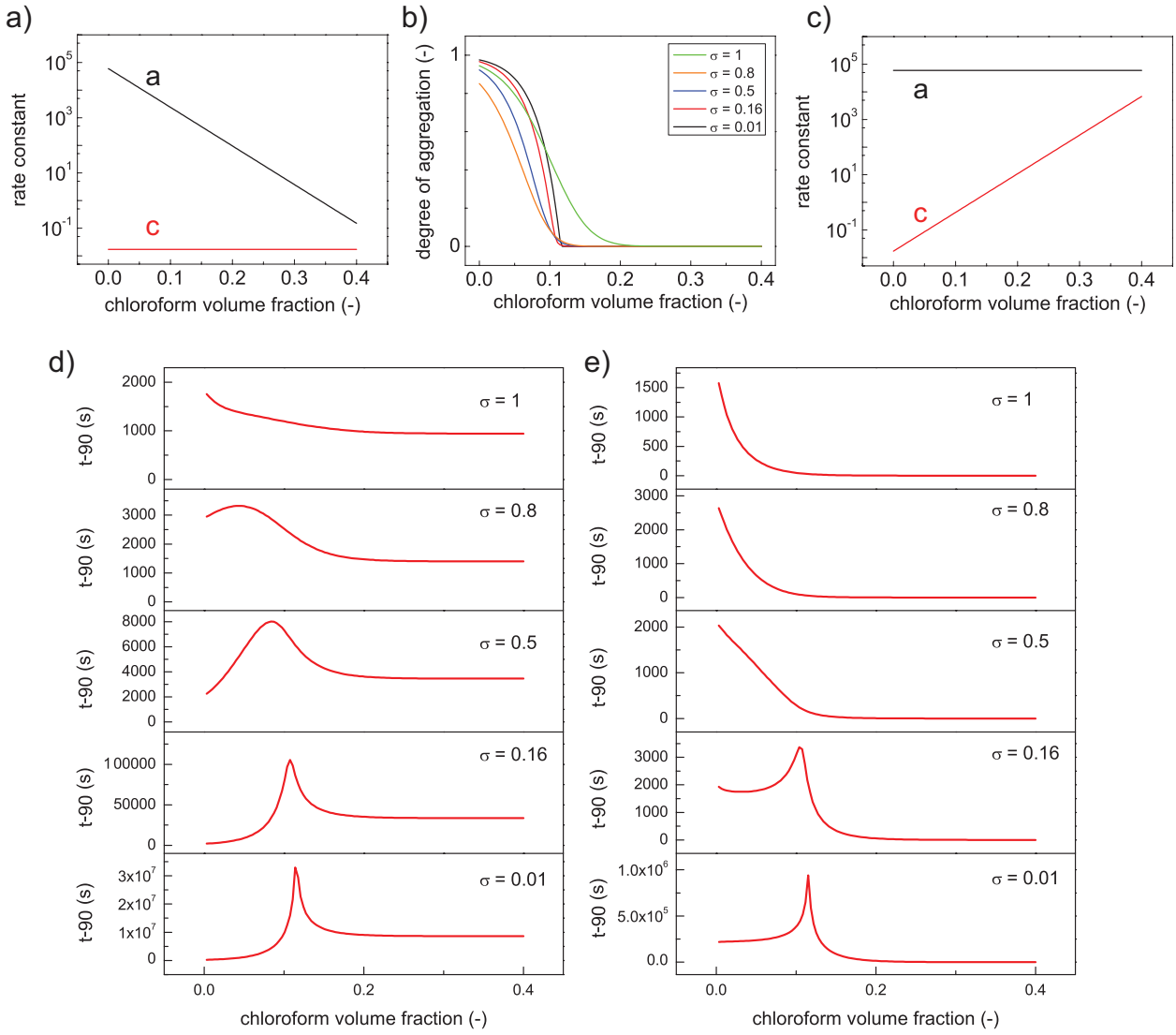

Figure S12. The influence of cooperativity σ on the depolymerization rate is assessed by performing simulations with the kinetic model. *t*-90 is followed as a function of chloroform volume fraction *f* for different values of σ, 1) for a mechanism in which the forward rate constant *a* decreases with *f* and backward rate constant *c* is solvent-independent (m_a = 14, m_c = 0, a) and 2) for a mechanism in which c increases with *f* and *a* is constant (m_a = 0, m_c = 14, c). As shown in pane d) (m_a = 14, m_c = 0) and e) (m_a = 0, m_c = 14), for both mechanisms a minimum rate is obtained around the critical chloroform volume fraction for small values of σ. In pane b), the degree of aggregation *vs.* chloroform volume fraction under equilibrium conditions is depicted for the different simulations. Details on simulations: $a^0 = 6 \cdot 10^4$ $M^{-1}s^{-1}$, $c^0 = 1.71 \cdot 10^{-2}$ s^{-1}, OPV dimer concentration = 12 μM. For the cooperative simulations, the nucleus size *n* equals 5. For the isodesmic simulations (σ = 1), all species P_i with $i \geq 2$ are taken into account for the calculation of the degree of aggregation and the depolymerization rate (*i.e.* *t*-90).

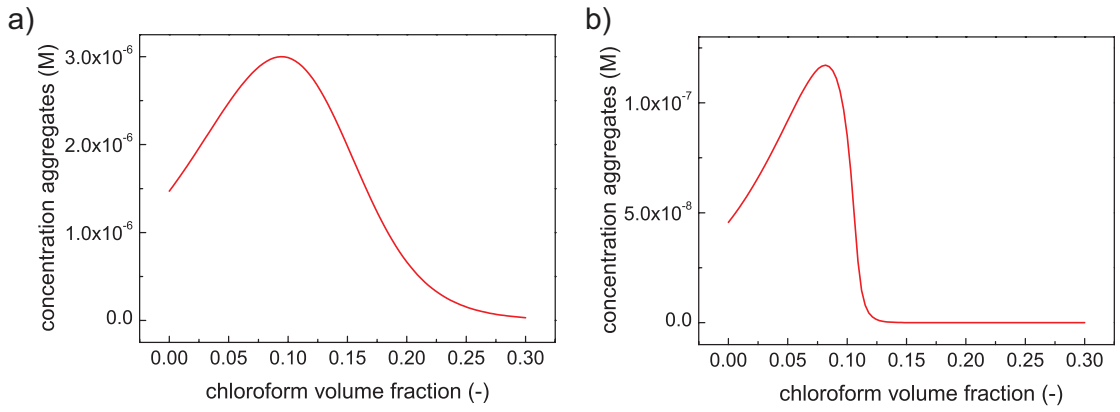

Figure S13. The total concentration of aggregates calculated as a function of chloroform volume fraction using the equilibrium model. For both an isodesmic (a) and a cooperative (b) aggregation mechanism, the total concentration of aggregates first increases with f and subsequently decreases at high values of f where the aggregates are completely depolymerized. The increasing total concentration of aggregates upon increasing f indicates that the short aggregates which are formed upon addition of chloroform cannot solely originate from partly depolymerized larger aggregates. Some of these short aggregates have to be formed by assembly starting from the monomeric state. The rate of this re-assembly process is very dependent on the cooperativity σ, as evidenced by kinetic simulations as outlined in Figure S15. Those simulations reveal a decreasing polymerization rate with decreasing σ. Hence, in a cooperative aggregation mechanism, *de novo* assembly of monomers released by depolymerization of long aggregates is very slow and limits the equilibration rate of the depolymerization process. This assembly process is slowed down upon increasing f, due to the decreasing forward rate constant a, the increasing backward rate constants b and c, or a combination of both. This results in a minimum rate at the critical chloroform volume fraction. Beyond the critical chloroform concentration, formation of aggregates *de novo* can be neglected and the equilibration rate of the depolymerization process is determined by the disassembly rate of large aggregates, which increase as a function of f for $f > f_{crit}$. Parameters used to calculate equilibrium concentrations: $K_e^0 = 3.5 \cdot 10^6$ M^{-1}; OPV dimer concentration = 12 μM; $m = 7.9 \cdot 10^4$ J/mol; isodesmic system $\sigma = 1$; cooperative system $n = 5$, $\sigma = 0.16$; for isodesmic system all species X_i with $i > 1$ are taken into account for the concentration of aggregates, for cooperative system all species X_i with $i > n$ are taken into account.

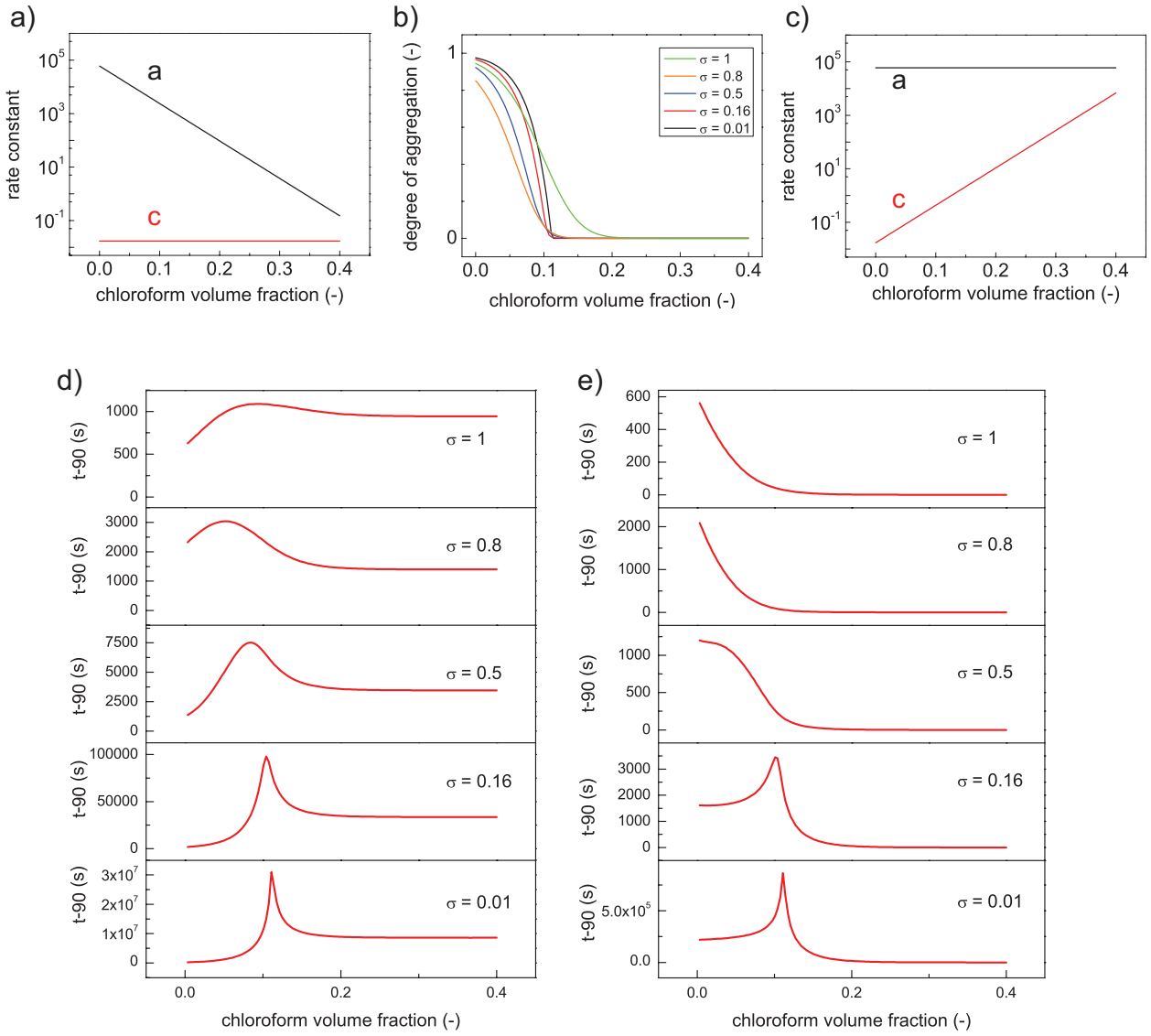

Figure S14. The influence of the free monomers in the chloroform phase on the observed depolymerization kinetics is assessed by performing simulations in which the depolymerization of assemblies in MCH is induced by the addition of *pure* chloroform. Analogous to Figure S12, both for (a) $m_a = 14$, $m_c = 0$ and (c) $m_a = 0$, $m_c = 14$, *t*-90 is followed as a function of chloroform volume fraction for different values of σ. As shown in pane d) ($m_a = 14$, $m_c = 0$) and e) ($m_a = 0$, $m_c = 14$), for both mechanisms a minimum rate is obtained around the critical chloroform volume fraction for small values of σ. Details on simulations: $a^0 = 6 \cdot 10^4$ $M^{-1}s^{-1}$, $c^0 = 1.71 \cdot 10^{-2}$ s^{-1}, OPV dimer concentration in pure MCH = 12 μM. For the cooperative simulations, the nucleus size n equals 5. For the isodesmic simulations ($\sigma = 1$), all species P_i with $i \geq 2$ are taken into account for the calculation of the degree of aggregation and *t*-90.

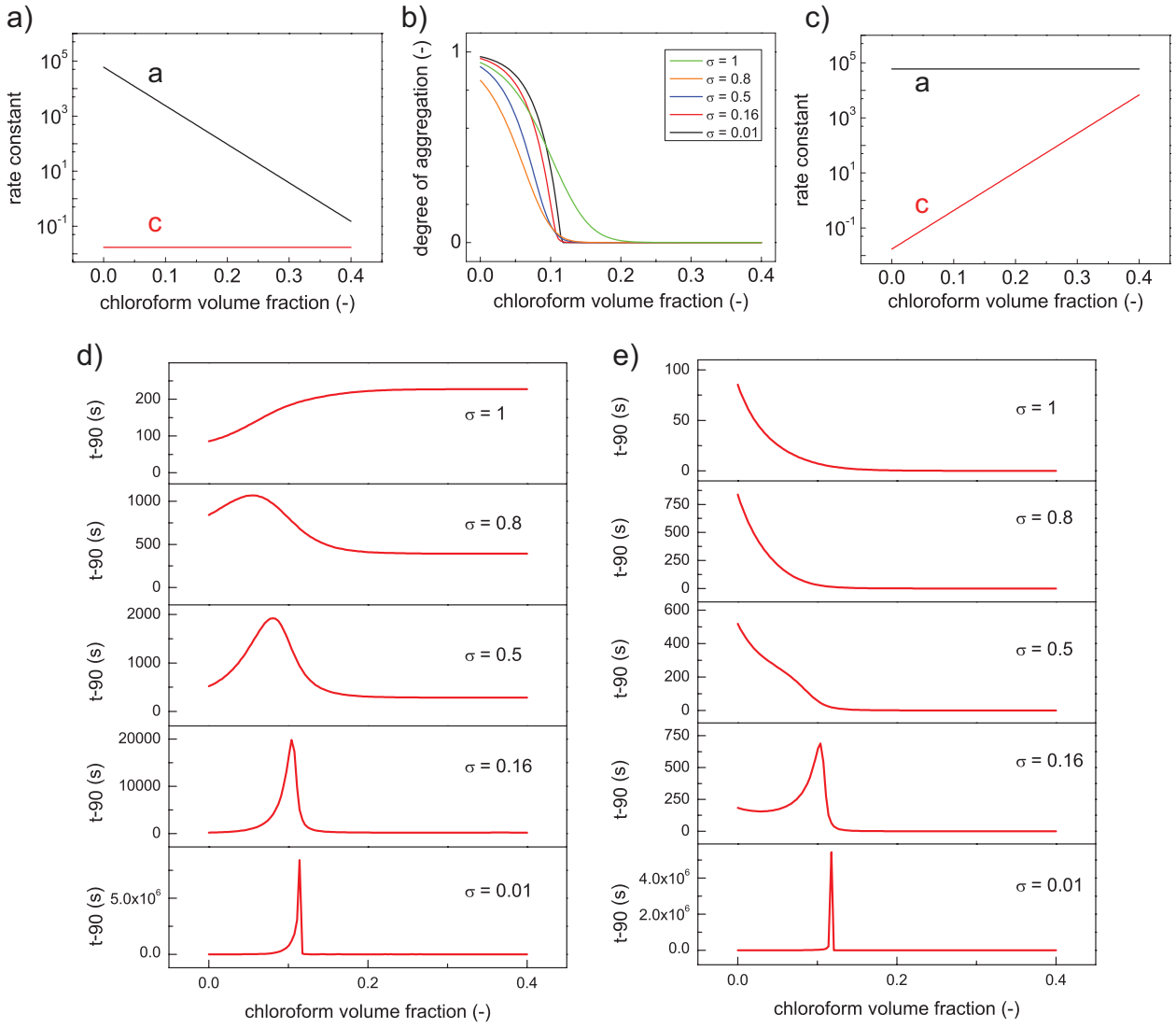

Figure S15. The influence of cooperativity σ on the aggregation rate is – in analogy to the simulations shown in Figure S12 – assessed by performing simulations with the kinetic model. The aggregation kinetics are simulated in different chloroform/MCH ratios starting from only free monomers. In agreement with the depolymerization simulations, the rate constants depend on the chloroform volume fraction as described in equations 2 – 4. *t*-90 is followed as a function of chloroform volume fraction f for different values of σ, 1) for a mechanism in which the forward rate constant a decreases with f and backward rate constant c is solvent-independent ($m_a = 14$, $m_c = 0$, a) and 2) for a mechanism in which c increases with f and a is constant ($m_a = 0$, $m_c = 14$, c). As shown in pane d) ($m_a = 14$, $m_c = 0$) and e) ($m_a = 0$, $m_c = 14$), for both mechanisms a minimum rate is obtained around the critical chloroform volume fraction for small values of σ. In pane b), the degree of aggregation *vs.* chloroform volume fraction under equilibrium conditions is depicted for the different simulations. Details on simulations: $a^0 = 6 \cdot 10^4$ $M^{-1}s^{-1}$, $c^0 = 1.71 \cdot 10^{-2}$ s^{-1}, OPV dimer concentration = 12 µM. For the cooperative simulations, the nucleus size n equals 5. For the isodesmic simulations ($\sigma = 1$), all species P_i with $i \geq 2$ are taken into account for the calculation of the degree of

aggregation and the aggregation rate (*i.e.* *t*-90). It should be noted that, although in reality no aggregates can be observed beyond the critical chloroform volume fraction, in these simulations a very small amount of aggregates is formed at high chloroform volume fractions, even if the degree of aggregation in figure b) is virtually zero. Based on this aggregation a *t*-90 value can be determined in the simulations at all chloroform volume fractions, even beyond the critical chloroform volume fraction.

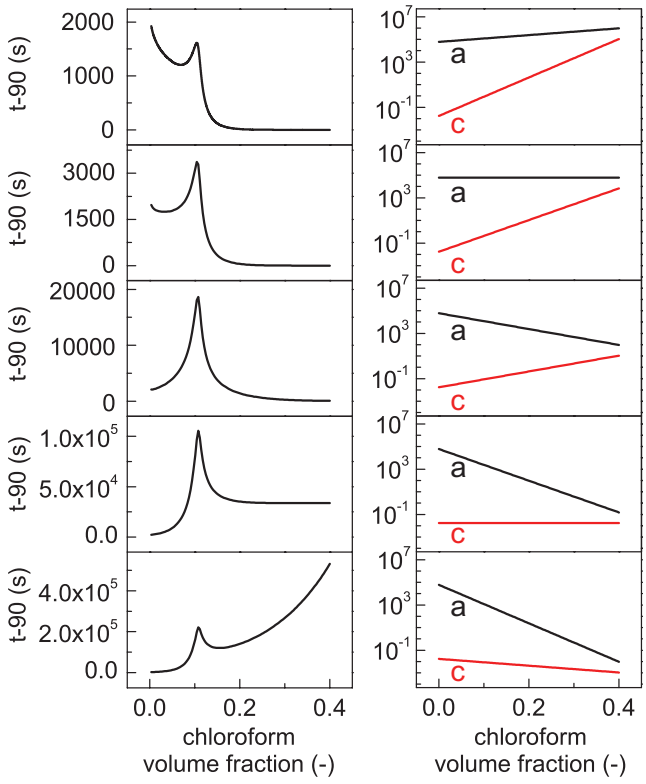

Figure S16. Depolymerization kinetics simulated with the kinetic nucleation-elongation model show that – analogous to the aggregation kinetics simulated in Figure 7 of the main text – if the slope of backward rate constant *c* as a function of *f* is less negative compared to the slope of forward rate constant *a* ($m_a + m_c > 0$), the minimum rate is obtained close to the critical solvent composition. The left pane shows the dependence of *t*-90 on *f* for the different relations between rate constants and solvent composition that are shown in the right pane. From top to bottom: $m_a = -3$, $m_c = 17$; $m_a = 0$, $m_c = 14$; $m_a = 7$, $m_c = 7$; $m_a = 14$, $m_c = 0$; $m_a = 17$, $m_c = -3$; rate constants are based on equations 2 – 4, $a^0 = 6 \cdot 10^4$ $M^{-1}s^{-1}$, $c^0 = 1.71 \cdot 10^{-2}$ s^{-1}, $\sigma = 0.16$, $n = 5$, OPV dimer concentration = 12 µM.

References

S1. Goldstein, R. F.; Stryer, L. *Biophys. J.* **1986**, *50*, 583-599.

S2. Jonkheijm. P.; van der Schoot, P.; Schenning, A. P. H. J.; Meijer, E. W. *Science* **2006**, *313*, 80-83.

S3. (a) Ashyraliyev, M.; Fomekong-Nanfack, Y.; Kaandorp, J. A.; Blom, J. G. *FEBS Journal* **2009**, *276*, 886-902. (b) Geier, F.; Fengos, G.; Felizzi, F.; Iber, D. Analysing and constraining signaling networks: parameter estimation for the user, in *Computational Modeling of Signaling Networks* (Editors Xuedong Liu, Meredith D. Betterton), **2012**, Humana Press.

S4. Korevaar, P. A.; George, S. J.; Markvoort, A. J.; Smulders, M. M. J.; Hilbers, P. A. J.; Schenning, A. P. H. J.; de Greef, T. F. A.; Meijer, E. W. *Nature*, **2012**, *481*, 492-496.